


Spectral properties of soft X-ray transient MAXI J0637–430 using AstroSat

NEAL TITUS THOMAS ¹

—

SHIVAPPA B. GUDENNAVAR ¹

—

RANJEEV MISRA²

—

BUBBLY S. G. ¹

—

¹*Department of Physics and Electronics, CHRIST (Deemed to be University)
Bangalore Central Campus, Bengaluru - 560029, India*

²*Inter-University Centre of Astronomy and Astrophysics
Post Bag 4, Ganeshkhind, Pune - 411007, India*

(Received : 22-10-2021; Accepted : 2-12-2021; Published : 3-2-2022)

Submitted to The Astrophysical Journal

ABSTRACT

Soft X-ray transients are systems that are detected when they go into an outburst, wherein their X-ray luminosity increases several orders of magnitude. These outbursts are markers of the poorly understood change in the spectral state of these systems from low/hard state to high/soft state. We report the spectral properties of one such soft X-ray transient: MAXI J0637–430, with data from the *SXT* and *LAXPC* instruments on-board *AstroSat* mission. The source was observed for a total of ~ 60 ks over two observations on 8th and 21st November, 2019 soon after its discovery. Flux resolved spectral analysis of the source indicates the presence of a multi-colour blackbody component arising from the accretion disk and a thermal Comptonization component. The stable low temperature (~ 0.55 keV) of the blackbody component, points to a cool accretion disk with an inner disk radius of the order of a few hundred km. In addition, we report the presence of a relativistically broadened Gaussian line at 6.4 keV. The disk dominated flux and photon power law index of $\gtrsim 2$ and a constant inner disk radius indicate the source to be in the soft state. From the study we conclude that MAXI J0637–430 is a strong black hole X-ray binary candidate.

Keywords: Accretion — X-ray binaries — Transients — Black Hole physics

1. INTRODUCTION

Soft X-ray transients are a subclass of low mass X-ray binaries (LMXBs) that appear as extremely faint sources ($L = 10^{30} - 10^{33}$ erg s⁻¹) during most of their lifetime. They are characterized by a non-steady transfer of mass onto the compact object and they occasionally undergo sporadic outbursts, which occur at intervals of 1 - 60 years (Chen et al. 1997; Tetarenko et al. 2016). This causes their X-ray luminosity to increase by a factor of upto 10^7 (Paradijs & McClintock 1995) which then decays back to quiescence with an e - folding timescale of ~ 30 days (Chen et al. 1997). During the

short outbursts, they emit enough X-rays, which makes them the brightest X-ray sources ($L = 10^{37} - 10^{38}$ erg s⁻¹) in the sky. The occurrence of these outbursts is attributed to instabilities in the accretion disk that are both viscous and thermal in nature (Meyer & Meyer-Hofmeister 1981; Cannizzo et al. 1995; King & Ritter 1998; Lasota 2001). Soft X-ray transients, especially the ones harbouring a black hole, usually go undetected; and are discovered only when they undergo an outburst.

MAXI J0637–430 is one such source, which was first detected by the *MAXI/GSC* nova alert system during seven scan transits from 2nd - 3rd November, 2019 in the 2 - 4 keV and 4 - 10 keV bands. The scans revealed the source to be located at RA (J2000) = 06 h 38 m 54 s, Dec (J2000) = -42 h 45 m 57 s in the soft band (2 - 4 keV) and at RA (J2000) = 06 h 37 m 43 s, Dec (J2000) = -43 h 03 m 15 s in

the hard band ($4 - 10 \text{ keV}$) with 90% confidence level (Negoro et al. 2019). Since its first detection, MAXI J0637–430 underwent a considerable increase in its flux from $59 \pm 6 \text{ mCrab}$ to $\sim 200 \text{ mCrab}$ in the $2 - 4 \text{ keV}$ band and from $32 \pm 6 \text{ mCrab}$ to $\sim 50 \text{ mCrab}$ in the $4 - 10 \text{ keV}$ band (Negoro et al. 2019). A Target of Opportunity (ToO) observation performed on 3rd November, 2019 by the *Swift* mission detected MAXI J0637–430 at RA (J2000) = 06 h 36 m 23.59 s, Dec (J2000) = $-42 \text{ h } 52 \text{ m } 04.1 \text{ s}$, which was consistent with MAXI’s hard band localization. Its X-ray spectrum modelled using absorbed disk blackbody + power law with inner disk temperature (kT_{in}) of $0.9 \pm 0.1 \text{ keV}$ and power-law index (Γ) of 2.3 ± 0.8 indicated that the source underwent an outburst and transitioned from hard to soft spectral state. An optical counterpart with a brightness of $u = 14.87 \pm 0.02$ (Vega) was detected by the *UVOT* instrument on-board *Swift* at RA (J2000) = 06 h 36 m 23.23 s Dec (J2000) = $-42 \text{ h } 52 \text{ m } 04.25 \text{ s}$. Since there are no known stars at this position, it was deemed that this optical source underwent a significant brightening, as is common for the optical counterpart of black hole low mass X-ray binaries (BH-LMXBs) during outbursts (Kennea et al. 2019). Follow up observation by the *NuStar* mission found the source to be at a flux of $\sim 95 \text{ mCrab}$. Preliminary analysis of spectrum of the source in the energy range $3 - 79 \text{ keV}$ with a thermal disk blackbody component, power law and a reflection component yielded a kT_{in} of $0.628 \pm 0.004 \text{ keV}$ and a Γ of 2.40 ± 0.04 (90% confidence errors) (Tomsick et al. 2019). MAXI J0637–430 was also observed in radio band with the *ATCA* with flux densities of $66 \pm 15 \mu\text{Jy}$ at 5.5 GHz and $60 \pm 10 \mu\text{Jy}$ at 9 GHz (Russell et al. 2019). However, as the nature of the radio jet emission could not be deciphered, the source could not be properly classified using the radio/X-ray correlation in X-ray binaries. The source was also observed in infrared band with the simultaneous imaging camera *SIRIUS* attached to 1.4 m telescope *Infrared Survey Facility (IRSF)*, where the estimated magnitudes in the J, H and K bands were 17.40 ± 0.01 , 17.69 ± 0.02 and 17.96 ± 0.05 , respectively (Murata et al. 2019). Spectral analysis of the X-ray data from *Swift* observations with an absorbed disk blackbody model showed the source to have a kT_{in} of $0.675 \pm 0.003 \text{ keV}$ (Knigge et al. 2019), which is consistent with the value obtained from *NuStar* observations. Since its discovery, MAXI J0637–430 was observed by the *NICER* mission continuously with a cadence of 1-2 days, which observed it undergo a spectral state transition. After ~ 23 days since its discovery, it was reported that source transitioned into the hard state (Remillard et al. 2020). Subsequent observations by *Swift* showed that MAXI J0637–430 could possibly be approaching its quiescence level (Tomsick & Lazar 2020). A multi-wavelength study of the source was carried out by Tetarenko et al. (2021) using data from *Swift-XRT* and *UVOT*, *Gemini/GMOS*, *ATCA* and *AAVSO*. This study made use of an irradiated accretion disk model - (*diskir*) (Gierliński et al. 2009) to derive the time-series evolution of its spectral parameters over the entire outburst cycle. Analysis of *NICER* data by (Jana et al. 2021) revealed the source to comprise of an ultra-soft thermal com-

ponent ($kT_{in} \lesssim 0.6 \text{ keV}$) and a power law tail. The study also showed that its spectra do not need a thermal component corresponding to the emission from neutron star surface, thus suggesting that the compact object in the MAXI J0637–430 is most likely a black hole. Mass of the black hole inferred from this study is $5 - 12 M_{\odot}$ for a source distance of $d < 10 \text{ kpc}$ and the distance to the source is found to have a lower limit of 6.5 kpc . Baby et al. (2021) found that the $0.5 - 25 \text{ keV}$ spectra of the source could be modelled with a multi-colour disc emission (*diskbb*) convolved with a thermal Comptonisation component (*thcomp*). Spectral fitting with the *kerbb* model in conjunction with the soft-hard transition luminosity, favour a black hole with mass between $3 - 19 M_{\odot}$ and retrograde spin at a distance $< 15 \text{ kpc}$. Broadband spectral study on *NuSTAR* data of the source showed that a two-component model, comprising of a combination of multi-colour disk blackbody and thermal Comptonization component is adequate to fit the spectra only upto 10 keV . When higher energies are considered, scenarios involving a plunging region and reprocessing of returning disk radiation are equally possible (Lazar et al. 2021).

Encouraged by the observation campaigns carried out by various satellite and ground based telescopes, ToO observations of MAXI J0637–430 were performed using the *Soft X-ray Telescope (SXT)* and *Large Area X-ray Proportional Counter (LAXPC)* instruments on-board *AstroSat* in the $0.3 - 80 \text{ keV}$ energy range on 8th and 21st November, 2019. Here, we report the results of spectral and temporal studies carried out on MAXI J0637–430 data from the *SXT* and *LAXPC* instruments. The details of *AstroSat* observations and the data reduction procedures are described in Section 2. In Section 3, lightcurve and hardness intensity diagram (HID) are presented. In Section 4, we present the results of spectral analysis. The findings and summary of the results are discussed in Section 5.

2. OBSERVATIONS AND DATA REDUCTION

ToO observations of MAXI J0637–430 (Thomas et al. 2019) in the $0.3 - 80 \text{ keV}$ energy range were carried out using *SXT* and *LAXPC* on-board *AstroSat* for a total of ~ 60 ks on 8th (hereafter, Observation 1), 15th and 21st November, 2019 (hereafter, Observation 2). We did not include the 15th November data in our study as it contains 9-pointing safety observations for the *UVIT* instrument on-board *AstroSat*, each with different pointing and offset. Due to this, the spectra from the individual pointing could not be combined as the effective area of the instrument changes with the offset. Moreover, since the *LAXPC* pointings were also different, flux measurement using *SXT+LAXPC* data could not be made. *AstroSat* observations used for our study, marked on the $2 - 20 \text{ keV}$ MAXI lightcurve in Figure 1 shows that Observation 1 was carried out shortly after the outburst peak, whereas Observation 2 was performed midway during the outburst decay. The Photon Counting mode (PC) was employed for observation with *SXT*, whereas for *LAXPC*, the observation was carried out in the Event Analysis Mode

(EA). A log of observations used for this study is given in Table 1.

SXT is a focusing telescope equipped with a Charged Coupled Device (CCD) camera that performs X-ray imaging in the 0.3 – 8.0 keV energy range with a spectral resolution of ~ 150 eV at 6 keV (Singh et al. 2016). *SXT* data of MAXI J06347–430 was processed using the standard *SXT* pipeline - AS1SXTLevel2-1.4b¹. This yielded Level 2 event files for individual orbits of the observation, which were then merged into one master event file using the *SXT* Event Merger Tool². The merged event file was then used to extract source images with the help of XSELECT V2.4k. The source was selected between the region of 8' and 5' (inner radius) for Observations 1 and 2, respectively, and 15' (outer radius) to reduce the effect of pile-up of the CCD. The response matrix³ and background⁴ files provided by the *SXT* Payload Operations Centre (POC) were used for the analysis. Off-axis Auxiliary Response File (ARF) was created with the *sxt_ARFModule*². *SXT* data in the range 0.5 – 5.0 keV for Region 1 and 3; and 0.5 – 4.8 keV for Region 2 were used (Figure 4) as the data quality above and below these energy ranges was poor.

LAXPC is a cluster of three co-aligned proportional counters (*LAXPC-10*, *LAXPC-20*, *LAXPC-30*) that operates in the 3 – 80 keV energy range with an absolute temporal resolution of 10 μ s (Yadav et al. 2016; Agrawal 2017; Antia et al. 2017). Data from *LAXPC* was processed with the *LAXPC-SOFT* (Format A)⁵ to obtain event files, Good Time Interval (GTI) files, lightcurves, source and background energy spectra, Response Matrix Files (RMF) and power density spectra. *LAXPC-20* data alone was used for our study as it was reported by the POC that *LAXPC-10* underwent an abnormal change in its gain on 28th March, 2018 and *LAXPC-30* was not operational during this time. Moreover, as the energy spectrum above 20 keV was background dominated, spectral studies using *LAXPC* were restricted to 4 – 20 keV energy range.

3. LIGHTCURVE AND HARDNESS INTENSITY DIAGRAM (HID)

Net lightcurves of the source were obtained in the 0.7 – 7.0 keV range from the *SXT* instrument; and 4.0 – 5.0 keV and 5.0 – 30.0 keV ranges from the *LAXPC* instrument. These lightcurves were binned to ~ 50 s. It is seen that during the beginning of the outburst decay i.e. in Observation 1, the source intensity remains fairly constant at ~ 30 counts/s and ~ 28 counts/s in the 4.0 – 5.0 keV (Panel 2 in Figure 2) and 5.0 – 30 keV (Panel 3 in Figure 2) ranges respectively. This then changes as the count rates in both energy ranges

increase by a small factor towards the end of the observation. This jump in the count rate is reflected in the hardness-time diagram too (Panel 4 in Figure 2). In comparison, the *LAXPC* net flux along with the hardness ratio is seen to decrease monotonically through the latter part of the outburst decay i.e. in Observation 2 (Panels 2, 3 and 4 in Figure 3). Using *LAXPC-20* data of both the observations, a combined, 50 s binned HID was generated with hardness defined as the ratio of counts in the 5.0 – 30.0 keV range to 4.0 – 5.0 keV range and intensity defined as the sum of counts in the 4.0 – 30 keV range. From the pattern traced by the HID, it is not possible to determine if the source showed characteristics of the q-diagram exhibited by BH-LMXBs (Remillard & McClintock 2006) or the Z or Atoll pattern exhibited by NS-LMXBs (Hasinger & van der Klis 1989). However, it is seen that the HID showed variability in hardness from ~ 0.9 to ~ 1.9 (Figure 4). Further, in order to investigate the hardness-intensity relation in energy range < 4 keV, data from the *SXT* instrument, corresponding to the three regions in the *LAXPC*-HID was used to generate an HID (Figure 5). The hardness of this *SXT*-HID was defined as the ratio of counts in the 1.0 – 7.0 keV range to 0.3 – 1.0 keV range and the intensity was defined as the sum of counts in the 0.3 – 7.0 keV range, for time corresponding to all the three regions from the *LAXPC*-HID. Regions 1 and 3 in this *SXT*-HID show variations in average flux and hardness, whereas Region 2 has too less data points to make a definitive conclusion.

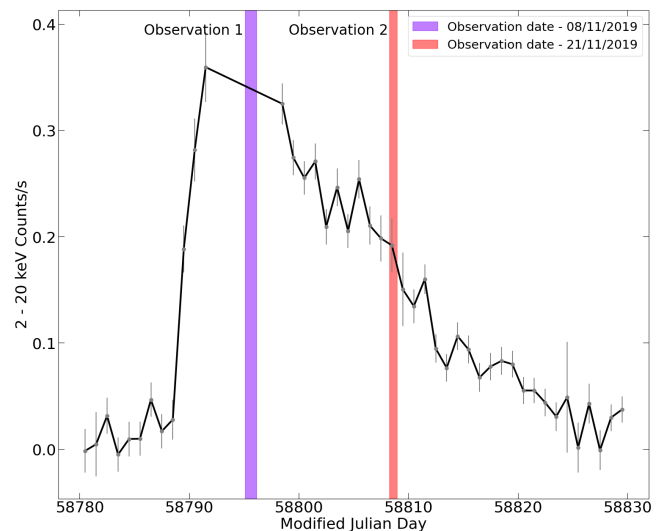


Figure 1. 1 day binned MAXI lightcurve of MAXI J0637–430 in 2 – 20 keV band

4. SPECTRAL ANALYSIS

The simultaneous broadband X-ray spectral coverage of *AstroSat* with the *SXT* and *LAXPC* instruments was used to perform flux resolved spectroscopy. This was done by dividing the *LAXPC*-HID into 3 regions: Region 1, 2 and 3. The divisions were made such that each region denotes an isolated

¹ https://www.tifr.res.in/~astrosat_sxt/sxtpipeline.html

² https://www.tifr.res.in/~astrosat_sxt/dataanalysis.html

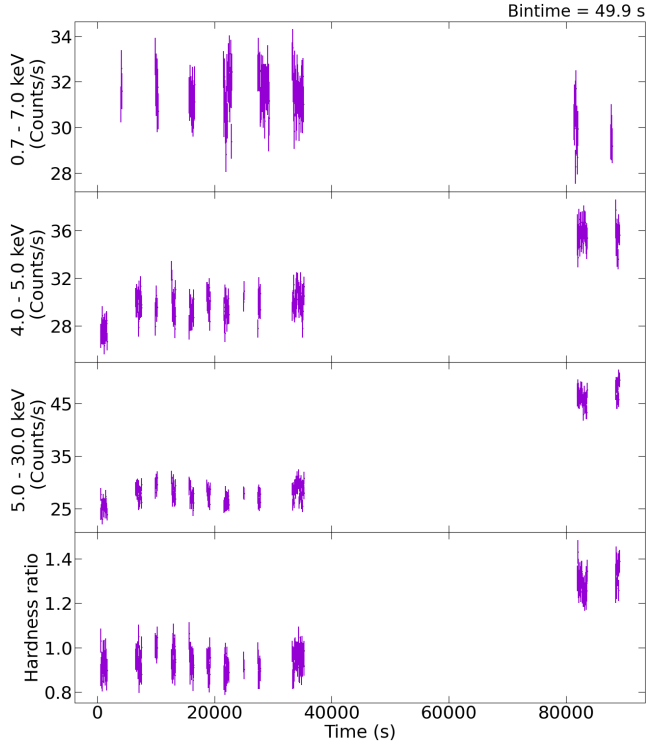
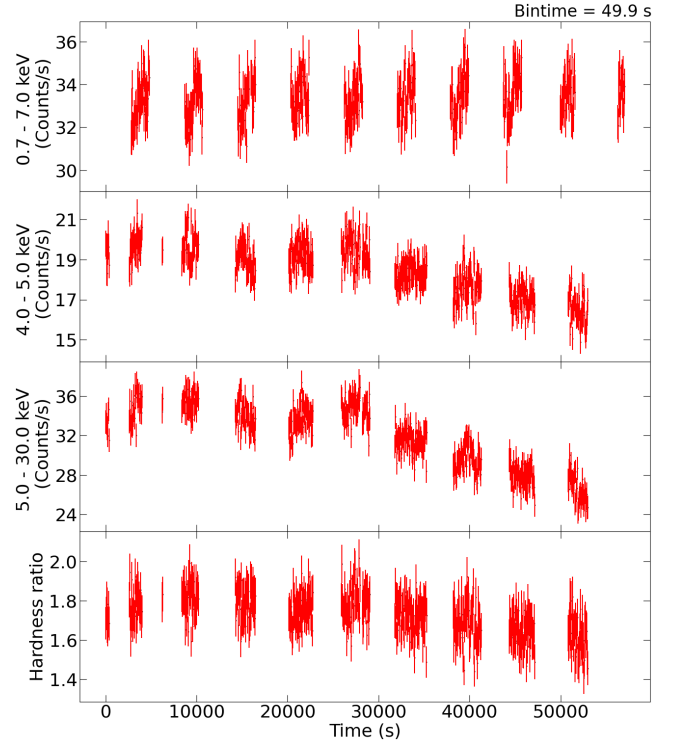
³ *sxt_pc_mat_g0to12.rmf*

⁴ *SkyBkg_comb_EL3p5_CLRd16p0_v01.pha*

⁵ <http://astrosat-ssc.iucaa.in/?q=laxpcData>

Table 1. Observation log

Obs. ID	Date	MJD	Exposure (ks)	
			SXT	LAXPC
9000003290	08-11-2019	58795	8.7	6.5
9000003328	21-11-2019	58808	19.1	24.8

**Figure 2.** *SXT* lightcurve of the source in 0.7 – 7.0 keV energy range (Panel 1), *LAXPC-20* net lightcurve in the energy ranges 4.0 – 5.0 keV (Panel 2) and 5.0 – 30 keV (Panel 3) and their hardness ratio (Panel 4) from Observation 1**Figure 3.** *SXT* lightcurve of the source in 0.7 – 7.0 keV energy range (Panel 1), *LAXPC-20* net lightcurve in the energy ranges 4.0 – 5.0 keV (Panel 2) and 5.0 – 30 keV (Panel 3) and their hardness ratio (Panel 4) from Observation 2

cluster of points in the *LAXPC-HID* (Figure 4). Simultaneous GTIs for both the *SXT* and *LAXPC* instruments were generated, using which simultaneous spectra for both instruments were generated for all three regions of the *LAXPC-HID*. The spectra were then fit with the spectral modelling tool XSPEC version : 12.10.1o (Arnaud 1996) in the energy ranges 0.5 – 5.0 keV from the *SXT* instrument for Regions 1 and 3; and 0.5 – 4.8 keV for Region 2; whereas from the *LAXPC* instrument, the energy range 4.0 – 20 keV was chosen for all three regions. These energy ranges were chosen as the spectra below 0.5 and above 4.8 keV (from the *SXT* instrument) showed very high residuals and that above 20.0 keV (from the *LAXPC* was dominated by the background. A multi-colour blackbody model - `diskbb` (Mitsuda et al. 1984), was used along with a convolution Comptonization model - `simpl` (Steiner et al. 2009), in order to explain the emission from the accretion disk and thermally Comptonized corona, respectively. The energy range for the spectral fits were extended using energies 0.01 100 500 log to sup-

ply an energy-binning array. To account for absorption in the interstellar medium, we used the Tuebingen-Boulder Inter-Stellar Medium absorption model - `tbabs`, with the solar abundance table given by Wilms et al. (2000). Further, a multiplicative constant factor was included to address uncertainties caused due to cross calibration of the *SXT* and *LAXPC* instruments. As prescribed by the POC, a systematic error of 3% was added to all spectral fit (Bhattacharya 2017). In addition to this, gain fit was performed for the *SXT* data to account for the non-linear change in the detector gain. Slope of the gain was frozen to 1 leaving the offset to vary. There were positive residuals around 6.4 keV indicating possible presence of a disk reflection feature. A Gaussian component with its line energy frozen at 6.4 keV was later added to account for this. The addition of the Gaussian component yielded a small change in $\Delta\chi^2$ from 1.03 and 0.92 to 1.0 and 0.76 in Regions 1 and 2 respectively; whereas for Region 3 it remained constant. The model combination - `constant * tbabs(simpl * diskbb + gaussian)`

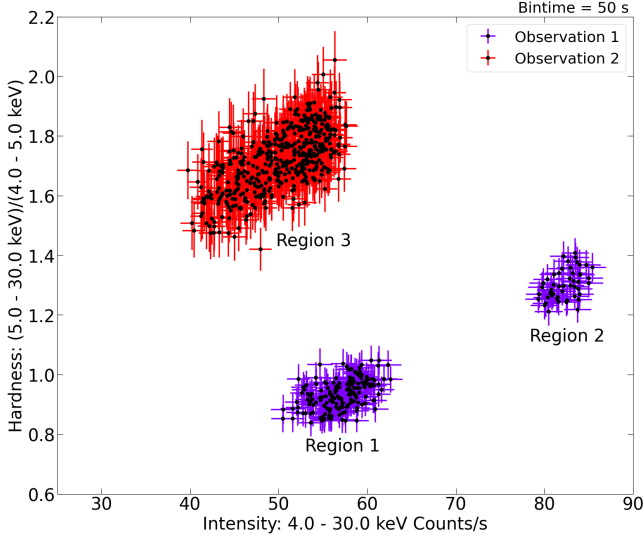


Figure 4. HID of the source from *LAXPC-20* data, which is divided into 3 regions for flux resolved spectral studies.

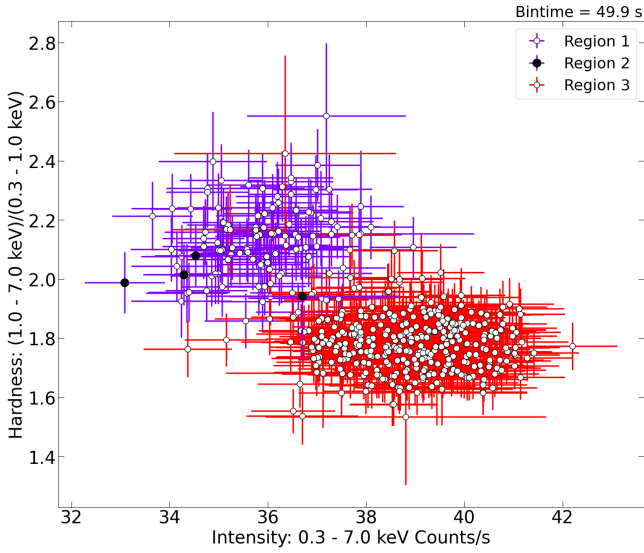


Figure 5. HID of the source from *SXT* data showing Regions 1, 2 and 3 as resolved in the *LAXPC*-HID.

yielded good fits for all the three regions, with $\Delta\chi^2$ of ~ 0.9 (Figure 6). The best fit spectral parameters of this fit are given in Table 2 and the corresponding spectra are give in Figure 6. The Norm of *diskbb* remains fairly constant in all the three regions. Hence, in order to understand the observed variation in the HID, spectral fit was repeated with the Norm of *diskbb* fixed at 2075. This value was obtained by fitting a constant through the Norms of all the three regions. Further, the unabsorbed total and disk flux were calculated in the 0.5 – 20 keV range using the *cflux* model. The best fit parameters of this spectral fit are given in Table 3.

In addition to this, we also carried out temporal analysis with

data from the *LAXPC* instrument in the 4 – 30 keV range. However, it did not yield substantial results.

5. RESULTS AND DISCUSSION

In this work, we analysed the *SXT* and *LAXPC* data from *AstroSat* observations (8th and 21st November, 2019) of MAXI J0637–430 in the 0.5 – 20 keV energy range. The analysis revealed three distinct clusters in the *LAXPC*-HID of the source (Figure 4). However, these clusters do not form a clear pattern to give insights regarding the exact nature of the source. Monitoring the source through its entire outburst cycle with *NICER* and *MAXI* has revealed its HID to exhibit signatures of the various states of a BH-LMXB in outburst (Jana et al. 2021; Baby et al. 2021). Flux resolved spectral analysis showed that the spectra can be characterized by a multi-colour blackbody component arising from the accretion disk along with a thermal Comptonization component. Our choice of model - *diskbb*, to characterise the soft component is in agreement with erstwhile studies carried out on the source. However, different models have been used to characterise its hard component - *powerlaw* (Tetarenko et al. 2021), *nthcomp* (Jana et al. 2021; Lazar et al. 2021) and *thcomp* (Baby et al. 2021). The accretion disk temperatures, 0.61, 0.65 and 0.52 keV in Regions 1, 2 and 3 respectively, point to a cool disk. This is in agreement with the studies carried out by Tetarenko et al. (2021), Jana et al. (2021) and Baby et al. (2021), where the disk temperature is seen to decay from ~ 0.6 to ~ 0.1 keV during the course of the outburst. The slightly lower value of disk temperature in Region 3 correlates with the region being harder in the HID (Figure 4). The *diskbb* Norms of 2103, 1455 and 2083 in Regions 1, 2 and 3, indicate constant accretion disk radius throughout both the observations which is consistent with that exhibited by many BH-LMXBs in the soft state (Done et al. 2007). Similar results have been found by Baby et al. (2021) who used the convolution model *thcomp* along with *diskbb* to characterise the *AstroSat* spectra of the source. Assuming a source distance of 10 kpc, inclination angle of 70° and a colour hardening factor of 1.7 (Shimura & Takahara 1995), we calculated the inner disk radius to be ~ 98 , ~ 81 and ~ 97 km in Regions 1, 2 and 3 respectively. For a black hole of 20 M_{\odot} , keeping the disk normalization constant at 2075, we estimated the inner disk radius to be $\sim 6 R_g$. This is the distance at which the Innermost Stable Circular Orbit (ISCO) is located for a non-rotating black hole. The increase in scatter fraction (obtained using *simpl* model) from $0.016^{+0.004}_{-0.003}$ in Region 1 to $0.031^{+0.01}_{-0.009}$ in Region 2 reflects the increased *LAXPC* count rate in the HID. In addition, the presence of a Gaussian line at 6.4 keV points to a reflection feature from the accretion disk. The width of this line (~ 1 keV in Regions 1 and 2) shows that it is broadened due to relativistic effects around the vicinity of the central compact object. It is to be noted that the width and the Norm of the Gaussian component is significantly smaller in Region 3. The unabsorbed total flux and disk flux of the source in the 0.5 – 20 keV range imply Eddington fraction of 0.025, 0.023 and 0.0141 for Regions 1, 2 and 3 respectively (Table 3). The ratio of

Table 2. Best fit model spectral parameters

Model	Parameter	Region 1	Region 2	Region 3
tbabs	$N_H(10^{20} \text{ cm}^{-2})$	3.300 ± 0.006	$2.120^{+0.045}_{-0.021}$	1.250 ± 0.005
simpl	Γ	$2.00^{+0.14}_{-0.16}$	$1.95^{+0.17}_{-0.20}$	2.46 ± 0.03
	$FracSctr$	$0.016^{+0.004}_{-0.003}$	$0.031^{+0.010}_{-0.009}$	$0.100^{+0.009}_{-0.008}$
diskbb	$kT_{in} \text{ (keV)}$	0.610 ± 0.005	0.650 ± 0.030	0.520 ± 0.007
	$Norm$	2103^{+165}_{-152}	1455^{+714}_{-465}	2083^{+104}_{-98}
Gaussian	$Line \text{ (keV)}$	6.4 (f)	6.4 (f)	6.4 (f)
	$Width \text{ (keV)}$	$1.06^{+0.35}_{-0.40}$	$1.49^{+0.42}_{-0.47}$	$0.20^{+0.56}_{-0.37}$
	$Norm \text{ (} 10^{-3} \text{)}$	$1.39^{+0.60}_{-0.50}$	$3.24^{+1.60}_{-1.40}$	0.34 ± 0.30
Reduced χ^2 / dof		1.03/363	0.76/109	1.33/460

Table 3. Best fit model spectral parameters with fixed diskbb Norm

Model	Parameter	Region 1	Region 2	Region 3
tbabs	$N_H(10^{20} \text{ cm}^{-2})$	3.31 ± 0.006	$3.87^{+0.04}_{-0.03}$	1.12 ± 0.005
simpl	Γ	$2.00^{+0.14}_{-0.16}$	$2.00^{+0.15}_{-0.17}$	2.49 ± 0.03
	$FracSctr$	$0.016^{+0.004}_{-0.003}$	0.028 ± 0.007	0.100 ± 0.008
diskbb	$kT_{in} \text{ (keV)}$	0.610 ± 0.003	0.620 ± 0.005	0.520 ± 0.005
	$Norm$	2075(f)	2075(f)	2075(f)
Gaussian	$Line \text{ (keV)}$	6.4(f)	6.4(f)	6.4(f)
	$Width \text{ (keV)}$	$1.06^{+0.35}_{-0.40}$	$1.32^{+0.34}_{-0.42}$	$0.37^{+0.56}_{-0.36}$
	$Norm \text{ (} 10^{-3} \text{)}$	$1.39^{+0.60}_{-0.50}$	$3.14^{+1.50}_{-1.30}$	$0.40^{+0.30}_{-0.20}$
Unabsorbed disk flux	$(10^{-9} \text{ erg cm}^{-2} \text{ s}^{-1})$	$5.31^{+1.05}_{-0.95}$	$4.77^{+1.20}_{-0.84}$	$2.58^{+1.05}_{-0.95}$
Unabsorbed total flux	$(10^{-9} \text{ erg cm}^{-2} \text{ s}^{-1})$	$5.53^{+1.05}_{-0.95}$	$5.15^{+1.18}_{-0.85}$	$3.07^{+1.04}_{-0.96}$
Unabsorbed disk flux/total flux		0.96	0.92	0.84
L/L_{Edd}		0.025	0.023	0.141
Reduced χ^2 / dof		1.02/364	0.77/110	1.34/461

unabsorbed disk flux to the total flux (~ 0.9) in all three Regions (Table 3), suggests that the total flux is dominated by emission from the accretion disk. This consistent disk dominated flux combined with the photon power law index of $\gtrsim 2$, across all the three regions of the HID, shows the source to be in soft state.

6. CONCLUSIONS

We carried out flux resolved spectral studies on two observations (~ 60 ks) of the soft X-ray transient source MAXI J0637 – 430 in the $0.5 - 20 \text{ keV}$ energy range using the *SXT* and *LAXPC* instruments on-board *AstroSat*. Spectral analysis shows the source to have a cool accretion disk having temperature $\sim 0.55 \text{ keV}$ with a reflection feature at 6.4 keV . The value of photon index of $\gtrsim 2$ and the ratio of unabsorbed disk flux to the total disk of ~ 0.9 points that MAXI J0637 – 430 was in the soft spectral state when observed by *AstroSat*. Also, it is seen that the value of the disk normalization is consistent with being constant (Table 2) and points to an accretion disk with an inner disk radius of $11.1 R_g$. This is ob-

served in several BH-LMXBs in the soft state. We conclude from our study that MAXI J0637–430 is a strong black hole X-ray binary candidate. Further observations and in-depth studies of the source during its future outbursts are essential to confirm its nature and unravel other physical parameters.

ACKNOWLEDGEMENTS

We thank the *SXT* POC at TIFR, Mumbai and for the *LAXPC* POC team for their support, timely release of data and providing the necessary software tools. This work has made use of software provided by HEASARC. The authors acknowledge the financial support of ISRO under *AstroSat* Archival Data Utilization Program (No. DS-2B-13013(2)/9/2019-Sec.2 dated April 29, 2019). This publication uses data from the *AstroSat* mission of the Indian Space Research Organisation (ISRO), archived at the Indian Space Science Data Centre (ISSDC). One of the authors (SBG) thanks the Inter-University Centre for Astronomy and Astrophysics (IUCAA), Pune for the Visiting Associateship.

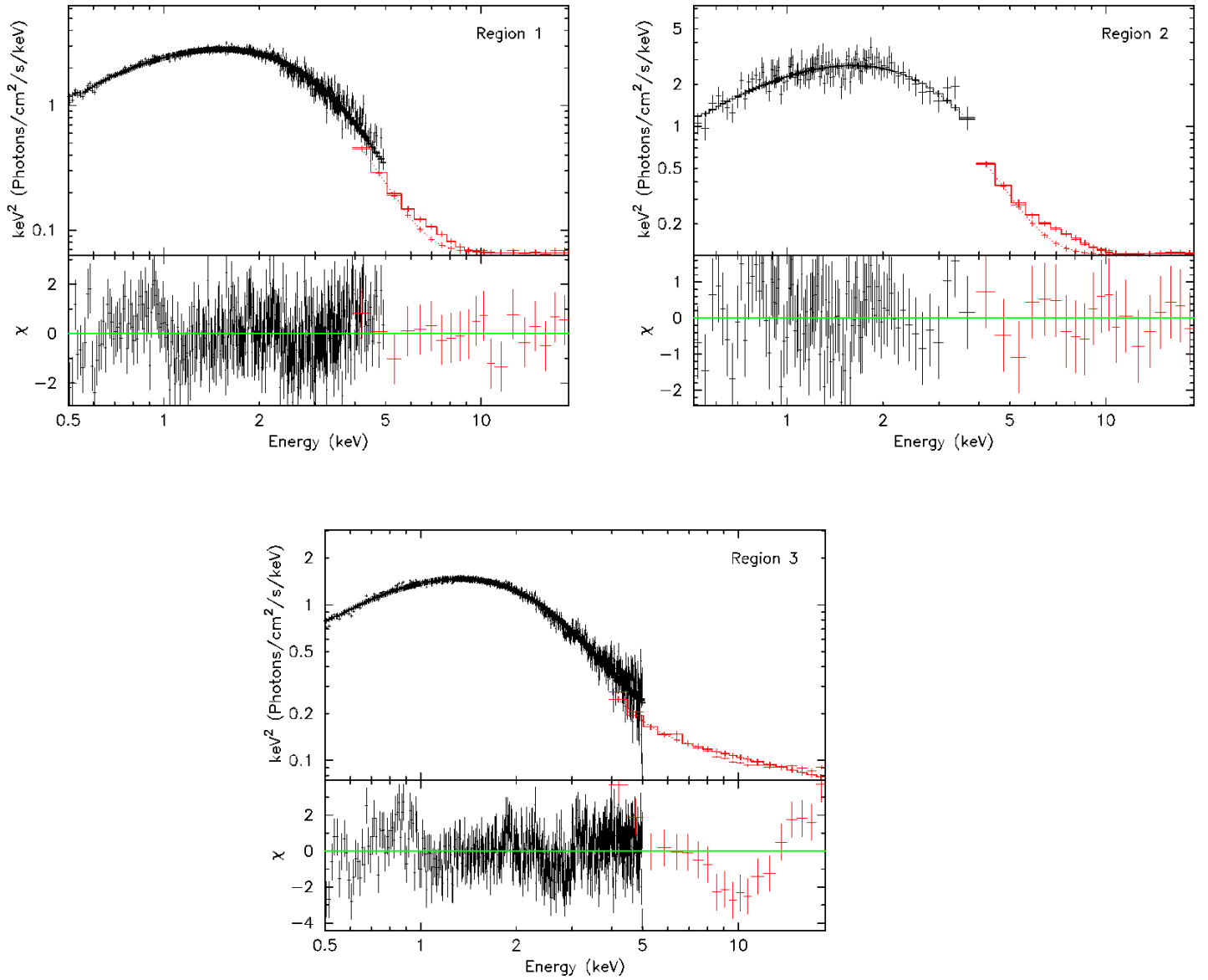


Figure 6. SXT+LAXPC unfolded spectra of Regions 1, 2 and 3 fit with the model combination $\text{constant} * \text{tbabs}(\text{simpl} * \text{diskbb} + \text{gaussian})$. The residuals ($\chi = (\text{data} - \text{model})/\text{error}$) are plotted in the bottom panels.

REFERENCES

Agrawal, P. 2017, *Journal of Astrophysics and Astronomy*, 38, doi: [10.1007/s12036-017-9449-6](https://doi.org/10.1007/s12036-017-9449-6)

Antia, H. M., Yadav, J. S., Agrawal, P. C., et al. 2017, *The Astrophysical Journal Supplement Series*, 231, 10, doi: [10.3847/1538-4365/aa7a0e](https://doi.org/10.3847/1538-4365/aa7a0e)

Arnaud, K. A. 1996, in *Astronomical Society of the Pacific Conference Series*, Vol. 101, *Astronomical Data Analysis Software and Systems V*, ed. G. H. Jacoby & J. Barnes, 17

Baby, B. E., Bhuvana, G. R., Radhika, D., et al. 2021, *MNRAS*, 508, 2447, doi: [10.1093/mnras/stab2719](https://doi.org/10.1093/mnras/stab2719)

Bhattacharya, D. 2017, *Journal of Astrophysics and Astronomy*, 38, 51, doi: [10.1007/s12036-017-9461-x](https://doi.org/10.1007/s12036-017-9461-x)

Cannizzo, J. K., Chen, W., & Livio, M. 1995, *ApJ*, 454, 880, doi: [10.1086/176541](https://doi.org/10.1086/176541)

Chen, W., Shrader, C. R., & Livio, M. 1997, *ApJ*, 491, 312, doi: [10.1086/304921](https://doi.org/10.1086/304921)

- Done, C., Gierliński, M., & Kubota, A. 2007, *A&A Rv*, 15, 1, doi: [10.1007/s00159-007-0006-1](https://doi.org/10.1007/s00159-007-0006-1)
- Gierliński, M., Done, C., & Page, K. 2009, *MNRAS*, 392, 1106, doi: [10.1111/j.1365-2966.2008.14166.x](https://doi.org/10.1111/j.1365-2966.2008.14166.x)
- Hasinger, G., & van der Klis, M. 1989, *A&A*, 225, 79
- Jana, A., Jaisawal, G. K., Naik, S., et al. 2021, *Monthly Notices of the Royal Astronomical Society*, 504, 4793, doi: [10.1093/mnras/stab1231](https://doi.org/10.1093/mnras/stab1231)
- Kennea, J. A., Bahramian, A., Evans, P. A., et al. 2019, *The Astronomer's Telegram*, 13257, 1
- King, A. R., & Ritter, H. 1998, *MNRAS*, 293, L42, doi: [10.1046/j.1365-8711.1998.01295.x](https://doi.org/10.1046/j.1365-8711.1998.01295.x)
- Knigge, C., Rao, A., Gandhi, P., & Altamirano, D. 2019, *The Astronomer's Telegram*, 13295, 1
- Lasota, J.-P. 2001, *New Astron. Rev.*, 45, 449, doi: [10.1016/S1387-6473\(01\)00112-9](https://doi.org/10.1016/S1387-6473(01)00112-9)
- Lazar, H., Tomsick, J. A., Pike, S. N., et al. 2021, *The Astrophysical Journal*, 921, 155, doi: [10.3847/1538-4357/ac1bab](https://doi.org/10.3847/1538-4357/ac1bab)
- Meyer, F., & Meyer-Hofmeister, E. 1981, *A&A*, 104, L10
- Mitsuda, K., Inoue, H., Koyama, K., et al. 1984, *PASJ*, 36, 741
- Murata, K. L., Adachi, R., Kawai, N., et al. 2019, *The Astronomer's Telegram*, 13292, 1
- Negoro, H., Miike, K., Nakajima, M., et al. 2019, *The Astronomer's Telegram*, 13256, 1
- Paradijs, J., & McClintock, J. 1995, *Optical and Ultraviolet Observations of X-Ray Binaries*, Cambridge University Press
- Remillard, R., Pasham, D., Gendreau, K., et al. 2020, *The Astronomer's Telegram*, 13427, 1
- Remillard, R. A., & McClintock, J. E. 2006, *ARA&A*, 44, 49, doi: [10.1146/annurev.astro.44.051905.092532](https://doi.org/10.1146/annurev.astro.44.051905.092532)
- Russell, T. D., Miller-Jones, J. C. A., Sivakoff, G. R., & Tetarenko, A. J. 2019, *The Astronomer's Telegram*, 13275, 1
- Shimura, T., & Takahara, F. 1995, *ApJ*, 445, 780, doi: [10.1086/175740](https://doi.org/10.1086/175740)
- Singh, K. P., Stewart, G. C., Chandra, S., et al. 2016, in *Space Telescopes and Instrumentation 2016: Ultraviolet to Gamma Ray*, ed. J.-W. A. den Herder, T. Takahashi, & M. Bautz, Vol. 9905, International Society for Optics and Photonics (SPIE), 389 – 398, doi: [10.1117/12.2235309](https://doi.org/10.1117/12.2235309)
- Steiner, J. F., Narayan, R., McClintock, J. E., & Ebisawa, K. 2009, *PASP*, 121, 1279, doi: [10.1086/648535](https://doi.org/10.1086/648535)
- Tetarenko, B. E., Shaw, A. W., Manrow, E. R., et al. 2021, *MNRAS*, 501, 3406, doi: [10.1093/mnras/staa3861](https://doi.org/10.1093/mnras/staa3861)
- Tetarenko, B. E., Sivakoff, G. R., Heinke, C. O., & Gladstone, J. C. 2016, *ApJS*, 222, 15, doi: [10.3847/0067-0049/222/2/15](https://doi.org/10.3847/0067-0049/222/2/15)
- Thomas, N. T., Gudennavar, S. B., Misra, R., & Bubbly, S. G. 2019, *The Astronomer's Telegram*, 13296, 1
- Tomsick, J. A., & Lazar, H. 2020, *The Astronomer's Telegram*, 13800, 1
- Tomsick, J. A., Garcia, J., Fabian, A., et al. 2019, *The Astronomer's Telegram*, 13270, 1
- Wilms, J., Allen, A., & McCray, R. 2000, *ApJ*, 542, 914, doi: [10.1086/317016](https://doi.org/10.1086/317016)
- Yadav, J. S., Agrawal, P. C., Antia, H. M., et al. 2016, in *Space Telescopes and Instrumentation 2016: Ultraviolet to Gamma Ray*, ed. J.-W. A. den Herder, T. Takahashi, & M. Bautz, Vol. 9905, International Society for Optics and Photonics (SPIE), 374 – 388, doi: [10.1117/12.2231857](https://doi.org/10.1117/12.2231857)